Kinetic Derivation of Aw-Rascle-Zhang-Type Traffic Models with Driver-Assist Vehicles

AgriEngineering

Article

Simplifying Field Traversing Efficiency Estimation Using Machine Learning and Geometric Field Indices

Gavriela Asiminari [1,2,3], Lefteris Benos [3], Dimitrios Kateris [3,*], Patrizia Busato [4], Charisios Achillas [1], Claus Grøn Sørensen [5], Simon Pearson [6] and Dionysis Bochtis [2,3,*]

[1] Department of Supply Chain Management, International Hellenic University, 57001 Thessaloniki, Greece; g.asiminari@certh.gr (G.A.); c.achillas@ihu.edu.gr (C.A.)
[2] farmB Digital Agriculture S.A., 17th November 79, 55534 Thessaloniki, Greece
[3] Institute for Bio-Economy and Agri-Technology (IBO), Centre for Research and Technology–Hellas (CERTH), 6th Km Charilaou-Thermi Rd., 57001 Thessaloniki, Greece; e.benos@certh.gr
[4] Interuniversity Department of Regional and Urban Studies and Planning (DIST), Polytechnic of Turin, Viale Mattioli 39, 10125 Torino, Italy; patrizia.busato@polito.it
[5] Department of Electrical and Computer Engineering, Aarhus University, 8000 Aarhus, Denmark; claus.soerensen@ece.au.dk
[6] Lincoln Institute for Agri-Food Technology (LIAT), University of Lincoln, Lincoln LN6 7TS, UK; spearson@lincoln.ac.uk
* Correspondence: d.kateris@certh.gr (D.K.); d.bochtis@certh.gr (D.B.)

Abstract: Enhancing agricultural machinery field efficiency offers substantial benefits for farm management by optimizing the available resources, thereby reducing cost, maximizing productivity, and supporting sustainability. Field efficiency is influenced by several unpredictable and stochastic factors that are difficult to determine due to the inherent variability in field configurations and operational conditions. This study aimed to simplify field efficiency estimation by training machine learning regression algorithms on data generated from a farm management information system covering a combination of different field areas and shapes, working patterns, and machine-related parameters. The gradient-boosting regression-based model was the most effective, achieving a high mean R^2 value of 0.931 in predicting field efficiency, by taking into account only basic geometric field indices. The developed model showed also strong predictive performance for indicative agricultural fields located in Europe and North America, reducing considerably the computational time by an average of 73.4% compared to the corresponding analytical approach. Overall, the results of this study highlight the potential of machine learning for simplifying field efficiency prediction without requiring detailed knowledge of a plethora of variables associated with agricultural operations. This can be particularly valuable for farmers who need to make informed decisions about resource allocation and operational planning.

Keywords: precision agriculture; coverage path planning; agricultural machinery; machine learning regression algorithms; predictive modeling; farm management information system (FMIS); computational time reduction

Academic Editors: Sotirios K. Goudos, Shaohua Wan and Achilles Boursianis

Received: 26 December 2024
Revised: 18 February 2025
Accepted: 6 March 2025
Published: 10 March 2025

Citation: Asiminari, G.; Benos, L.; Kateris, D.; Busato, P.; Achillas, C.; Grøn Sørensen, C.; Pearson, S.; Bochtis, D. Simplifying Field Traversing Efficiency Estimation Using Machine Learning and Geometric Field Indices. *AgriEngineering* **2025**, *7*, 75. https://doi.org/10.3390/agriengineering7030075

1. Introduction

An operational system in agriculture involves different components that influence its productivity, such as field characteristics, machinery, and other operational features, including traversing directions and field-work patterns [1]. For instance, the width of the equipment, the speed of operations, and the direction of travel can significantly affect how

well a field is worked, influencing both productivity and operational costs [2,3]. Optimized machine movement also plays a critical role in improving agricultural operations, as seen in navigation-based path planning [4] and robotic path optimization, where reducing traversal distances helps minimize computational overhead [5,6]. Among these factors, the shape of the field plays a very important role, as irregular shapes often require additional maneuvers which reduce field efficiency [7–10].

In general, field efficiency is considered a key indicator of machinery performance during field operations, representing the ratio of a machine's actual productivity to its theoretical maximum productivity [11–15]. This metric is crucial, as it has an important impact on the economic outcomes of agricultural operations [16]. A higher field efficiency translates to better resource utilization, minimizing waste, reducing operational costs, and ultimately improving profitability. From an environmental perspective, improving FTE can help lower carbon emissions, reduce soil compaction and erosion, and minimize chemical runoff, all while conserving energy [17,18].

The average norms used to quantify the field efficiency of precision agricultural machinery operations have several limitations, as they often lack specificity, failing to account for variability within a field, which leads to generalized results which may not accurately reflect performance in specific areas. This can result in overgeneralization, which may not capture the true efficiency of machinery operations in diverse and complex agricultural environments. To address these challenges, several studies have developed various field indices. The importance of field shape in determining efficiency was emphasized in [19], using basic shape descriptors for object identification, namely convexity, compactness, principal axes, and elliptic and circular variance. Additionally, the perimeter-to-area (P/A) ratio was also suggested in [10,20]. The impact of several shape indices on field efficiency was also evaluated, through linear regression models, by Amiama et al. [21]. Gonzalez et al. [22] developed an efficiency index considering both the size and shape of fields, specifically intended for integration into a geographic information system (GIS) for computer-based analysis. In the same vein, Al-Amin et al. [15] developed algorithms to assess field efficiency based on the size and shape of the fields while also adding economic analysis. Zandonadi et al. [23] investigated combined effects of field size, field shape, and implement width for estimating off-target application regions.

Zhou et al. [24] introduced an objective index for field efficiency, known as field traversing efficiency (FTE). This metric is based on the distance covered by agricultural machinery during field operations and is defined by specific, quantifiable operational parameters. Different combinations of field, machine, and operating features were examined. It was deduced that odd field shapes tend to have lower average values of FTE compared to more regular shapes. Moreover, AB (straight parallel passes) and BL (first turn skip) field-work patterns were more effective than the SF (skip and fill) pattern. Driving in the 90° direction also produced a higher average FTE than the other tested directions, while shorter machine operating widths resulted in a higher productive traveled distance.

Although the FTE approach represents an objective metric for the operational efficiency of a field area, its calculation involves multiple geometric and spatial processing steps that require high computational requirements. Specifically, the process involves determining working and non-working distances by generating field coverage patterns and defining traversal paths. Since FTE is calculated multiple times for the same field under different working widths, turning radii, and traversal directions [25], the processing time increases significantly, making large-scale evaluations even more demanding. To address this issue, a machine learning (ML)-based approach could make the FTE estimation more efficient, reducing computational time while maintaining accuracy and reliability, by leveraging advancements in regression ML algorithms [26,27].

The primary scope of this study is to develop an efficient, large-scale FTE estimation method that can be applied at both the production and regional levels. Unlike traditional methods which are computationally intensive, this ML-driven approach offers rapid estimation without compromising accuracy. Multiple ML regression models were trained on data from 4000 fields generated via a farm management information system (FMIS). The key innovation lies in utilizing shape indices, simple yet informative geometric descriptors, as inputs for ML models to predict FTE, eliminating the need for time-consuming analytical calculations. Overall, this approach simplifies field efficiency estimation for farmers and agronomists by eliminating complex calculations. It has the potential to optimize resource allocation, improve operational planning, and lead to cost savings, while enhancing sustainability, particularly in terms of energy consumption, labor, and equipment wear, making it ideal for both small and large operations.

2. Materials and Methods

2.1. Data Acquisition

The field-related data used for training the ML regression algorithms in this research were obtained through a systematic process that involved the following: (a) the collection of field data; (b) the computation of field indices associated with field geometry; and (c) the average FTE estimation per field. A total of 4000 fields were considered in this analysis, with a minimum area of approximately 1 ha and a maximum area of approximately 30 ha. Overall, the dataset contained a wide range of field sizes, with approximately 40% of fields below 5 ha, 30% between 5 and 15 ha, and 30% above 15 ha. Smaller fields were more abundant in our dataset, since they are often more irregular in shape, affecting field efficiency. However, despite smaller fields being more common, the dataset still included a good mix of relatively medium and large fields, ensuring a balanced representation. In addition, the fields covered a wide range of agricultural landscapes. This diverse dataset allowed for a thorough evaluation of the ML models' performance across different field sizes and types, contributing to effectively handling diverse agricultural scenarios, thus making the results more applicable to real-world situations.

To create a dataset from real fields of different shapes and sizes, an FMIS (farmB digital agriculture S.A., Thessaloniki, Greece) was utilized, which used application programming interface (API) calls to automate the collection process. In addition, the coordinates of the field boundaries and the area of each field were acquired from a GIS database supported by the FMIS. The FMIS also provided a user interface to depict field boundaries in order to select fields with different shapes and sizes.

2.2. Calculation of Geometric Field Indices

Once the field boundaries were acquired, a variety of geometric indices were calculated to determine the shape of each field, as the FTE is strongly affected by this factor. Fields with more regular, compact shapes tend to be more efficient in machinery-based operations with fewer turns and overlaps, leading to a higher FTE. In contrast, fields with irregular shapes require more complex movements, leading to lower values of FTE [24,28,29]. The indices selected in this study were convexity, ellipticity, compactness, perimeter-to-area ratio, rectangularity, square-perimeter index, and average curb index, which are briefly described in Table 1.

Table 1. Geometric indices used in the present analysis.

Geometric Index	Definition	Formula
Convexity	Measures how closely the shape approximates its convex hull	$C = \frac{A_f}{A_h}$
Ellipticity	Evaluates how closely the field shape approximates an ellipse using the concept of moment invariants	$E_1 = \begin{cases} 16\pi^2 I_1, \ if \ I_1 \leq \frac{1}{16\pi^2} \\ \frac{1}{16\pi^2 I_1}, \ otherwise \end{cases}$ $with: \ I_1 = \frac{\mu_{20}\mu_{02} - {\mu_{11}}^2}{{\mu_{00}}^4}$
Compactness	Measures how close the shape of a field is to a circle	$\kappa = \frac{4\pi A_f}{P_f^2}$
Perimeter-to-Area Ratio	Compares the perimeter to the area, providing a measure of shape complexity or boundary irregularity	$P/A \ ratio = \frac{P_f}{A_f}$
Rectangularity	Measures how closely the shape resembles a rectangle	$R = \frac{A_f}{A_r}$
Square-Perimeter	Relates a field's perimeter to the perimeter of a square of the identical area	$SPI = \frac{\sqrt[4]{A_f}}{P_f}$
Average Curb	Indicates the impact of headland area on the overall efficiency	$Ic, \ x = \frac{A_f - A_p}{Af}$

A_f: field area; A_h: area of field convex hull; A_p: area of inner polygon; A_r: area of field bounding box; I_1: first moment invariant; P_f: field perimeter; μ_{00}: the zeroth moment, representing the area of the shape; and μ_{20}, μ_{02}, μ_{11} : the second-order central moments, capturing the spread of the shape in different directions.

To provide a comprehensive assessment, $Ic, \ x$ was calculated for 144 different combinations of operational widths, turning radii, traversing directions, and field-work patterns summarized in Table 2, while the average $Ic, \ x$ was computed by taking the mean of curb indices across all combinations. The configurations included the following:

- Large-sized machinery with a minimum turning radius of 6 m and operating widths of 4.5 m to 12 m;
- Mid-sized machinery with a turning radius of 4.5 m and widths of 4.5 m to 9 m;
- Small-sized machinery with a turning radius of 3 m and widths of 3 m to 6 m.

Table 2. Combinations of operation widths, turning radii, and traversing directions for the calculation of $Ic, \ x$.

Minimum Turning Radius (m)	Operating Width (m)					Traversing Direction				Field-Work Patterns		
6	4.5	7.5	9	10.5	12	1	2	3	4	AB	SF	BL
4.5	4.5	6	7.5	9	-	1	2	3	4	AB	SF	BL
3	3	4.5	6	-	-	1	2	3	4	AB	SF	BL

Each configuration was evaluated using four traversing directions, defined based on the four largest sides of the field polygon. Additionally, three field-work patterns were applied to each scenario [25]:

- AB pattern: A straightforward patter with consecutive adjacent tracks;
- SF pattern: A "Skip and Fill" pattern where tracks are skipped and later covered optimizing turns;
- BL pattern: A "First Turn Skip" pattern designed to reduce non-working distance.

2.3. Calculation of Average Field Traversing Efficiency

As highlighted above, the FTE is a measure that reflects the effectiveness of field operations by comparing the working distance to the total distance covered during field work [24]. Unlike other field efficiency metrics which are affected by unpredictable factors, the FTE is defined by well-defined characteristics, including field shape, operation width, and the minimum turning radius of the vehicle. This makes FTE a useful indicator that

provides information on how well a vehicle will work in a field. The mathematical formula of FTE is given below:

$$FTE = \frac{\sum_{i=1}^{h} d(H_i) + \sum_{i=1}^{n} d(T_i)}{d(p)}, \quad (1)$$

where $\sum_{i=1}^{h} d(H_i)$ denotes the total length of all headlands passes and $\sum_{i=1}^{n} d(T_i)$ is the total length of tracks. The total length of the path is denoted by $d(p)$, including the length of turns and the length of moving from one sub-field to another.

In the original methodology presented in [24], driving directions were defined at angles of 0°, 30°, 60°, and 90° to evaluate the impact on efficiency. However, in this study, traversing directions were redefined based on the largest sides of the polygon rather than fixed angles. In particular, traversing directions aligned with the four longest sides of the field polygon. Defining directions based on the field's largest sides is easier for automated machinery systems than calculating precise angular directions. Furthermore, this modification provided practical advantages and was closer to real-word conditions.

To compute FTE efficiently, a route-planning algorithm was applied to generate optimal traversal paths for different combinations of parameters. The 144 combinations presented in Table 2 were tested for the calculation of FTE, showing how various operational configurations affected efficiency. The route-planning algorithm is an integral module of the FMIS, providing optimized field coverage, adaptability to field conditions, and decision support [25]. This algorithm takes into account field shape, machinery turning radius, operating width, traversing direction, and field-work patterns to create efficient traversal paths and minimize non-working distances such as turns. After the creation of paths, FTE was calculated for each combination based on Equation (1). To provide a better understanding of performance, the average FTE was computed from all the scenarios. This average FTE is a general efficiency indicator, giving some insight into how well a vehicle performs under different field and operational conditions.

2.4. Data Preprocessing

The resulting dataset, containing all the calculated geometric field indices and average FTE of the 4000 fields, was split into two parts: a training set, which consisted of examples for model training, and a testing set, used to evaluate the model's performance. In particular, an 80/20 ratio was selected for training and testing. Having the majority of field indices within the 0–1 range was suitable for ML models, as it simplified the modeling process by minimizing potential biases and enhancing the model's ability to generalize across diverse datasets. Only the ellipticity index needed to be normalized, thus ensuring uniformity in the data scale.

2.5. Field Traversing Efficiency Prediction Through Machine Learning

2.5.1. Tested Machine Learning Regression Algorithms

Seven ML algorithms commonly used in the relative literature [26,30–34] were trained to predict FTE, using the aforementioned geometric field indices: linear regression (LR), ridge regression (RR), decision tree regressor (DTR), random forest regressor (RFR), gradient-boosting regressor (GBR), support vector regressor (SVR), and XGBoost regressor (XGB). Their characteristics are as follows:

- The LR model is one of the most fundamental approaches for predicting quantitative responses by searching linear relationships between the independent and dependent variables;
- RR is a statistical technique used to reduce the coefficients of the regression by imposing a penalty on the absolute values of these coefficients to overcome the problem of multicollinearity;

- DTR segments the predictor space into regions based on decision rules to better handle non-linear relationships between variables, while their performance can be enhanced by aggregating multiple trees;
- RFR is an ensemble algorithm that predicts continuous values by averaging multiple decision trees, improving accuracy and reducing overfitting;
- GBR is an ensemble algorithm that predicts continuous values by sequentially combining multiple weak learners, typically decision trees, to improve accuracy and reduce errors;
- SVR predicts continuous values by minimizing errors within a defined margin, using a subset of training data (called support vectors) to capture complex, non-linear relationships;
- XGB is a fast, efficient gradient-boosting algorithm that predicts continuous values by combining multiple decision trees, ideal for large datasets.

2.5.2. Performance Metrics

Each model was separately trained using the produced training set. The goal was to find the best fitted model that adequately predicts average FTE values, avoiding overfitting. To improve the reliability of the models, 5-fold cross-validation was carried out. With the completion of the cross-validation, the performance of the following metrics was averaged:

- The mean error (ME) represents the average difference between the actual and predicted values:

$$ME = \frac{\sum_{i=1}^{n}(y_i - \hat{y}_i)}{n}. \quad (2)$$

- The mean absolute error (MAE) is defined as the absolute difference between the actual and predictable values:

$$MAE = \frac{\sum_{i=1}^{n}|y_i - \hat{y}_i|}{n}. \quad (3)$$

- The mean squared error (MSE) measures the average squared difference between and actual and predicted values:

$$MSE = \frac{\sum_{i=1}^{n}(y_i - \hat{y}_i)^2}{n}. \quad (4)$$

- The root mean square error (RMS) is the square root of the average squared differences between actual and predicted values:

$$RMS = \sqrt{\frac{\sum_{i=1}^{n}(y_i - \hat{y}_i)^2}{n}}. \quad (5)$$

- The normalized root mean square error ($nRMS$) normalizes RMS by the range of actual values, providing a scale-independent measure of error:

$$nRMS = \frac{RMS}{y_{max} - y_{min}} \times 100. \quad (6)$$

- R-squared (R^2) is a statistical measure that indicates the proportion of the variance in the dependent variable that is predictable from the independent variables:

$$R^2 = 1 - \frac{\sum_{i=1}^{n}(y_i - \hat{y}_i)^2}{\sum_{i=1}^{n}(y_i - \overline{y})^2}. \quad (7)$$

In the above equations, n represents the total number of data points, $\overline{y}$ is the mean of the actual values, $\hat{y}_i$ is the predicted value of the i^{th} data point, and y_i is the actual value of the i^{th} data point. Lastly, y_{max} and y_{min} refer to the maximum and minimum values of the actual data.

2.5.3. Summary of the Proposed Machine Learning-Based Workflow

Figure 1 presents a flowchart that outlines the typical ML-based workflow, beginning with the acquisition of field data. These data are then processed to extract geometric indices and calculate the average FTEs using Equation (1). The resulting dataset undergoes cleaning and preparation to ensure consistency and suitability for the ML model, which ultimately enhances its performance and accuracy. The preprocessed data are used to train the ML model, with the optimal parameters determined through 5-fold cross-validation. The final step evaluates the trained model's performance in predicting FTE on test data, which remain unseen during the training phase, ensuring an unbiased assessment of its predictive capabilities.

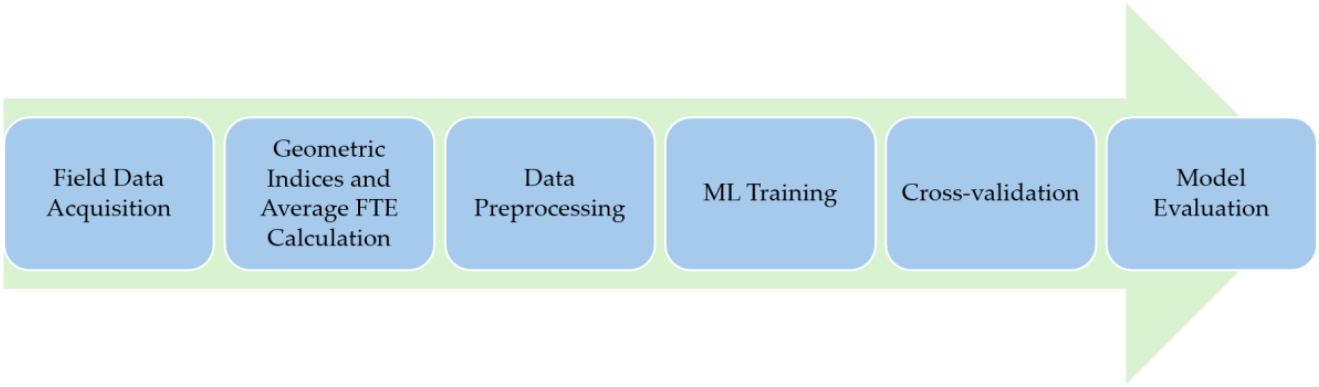

Figure 1. Schematic of the machine learning (ML)-based workflow of the present study.

2.6. Test of the Developed Model for Fields from Different Geographical Regions

After selecting the best tested ML regression algorithm for predicting FTE, the impact of the shape of a field on the FTE was assessed. To this end, fields with various shapes from seven different regions were examined. The following regions were selected, as they represented irregularly (Limburg, The Netherlands; Crete, Greece; Peloponnese, Greece; Monsanto, Portugal) and regularly shaped fields (Magnesia, Greece; Indiana, USA; Aarhus, Denmark). The dataset included 20 fields from each region, except for Magnesia, Greece, which comprised 35 fields, due to the availability of a larger number of fields in that particular area for data collection. Topographic maps of these regions are provided in Figure 2, with the yellow markers representing specific fields of interest. For each region, the average FTEs predicted by the ML-grounded model, based on field shape indices, were also compared with those calculated by Equation (1) to demonstrate potential limitations of the approach.

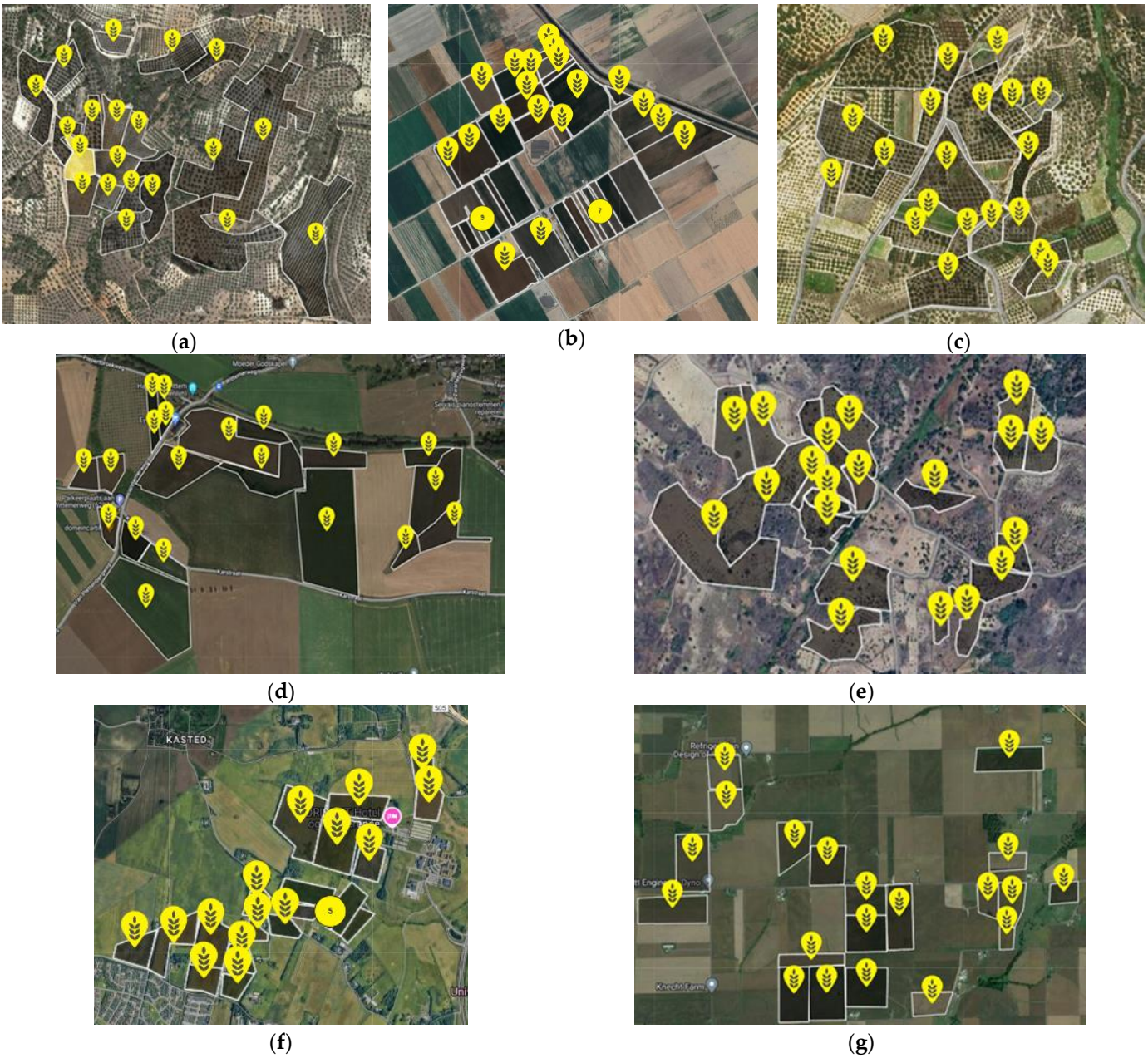

Figure 2. Fields inspected across different regions: (**a**) Peloponnese, Greece; (**b**) Magnesia, Greece; (**c**) Crete, Greece; (**d**) Limburg, The Netherlands; (**e**) Monsanto, Portugal; (**f**) Aarhus, Denmark; (**g**) Indiana, USA.

3. Results

3.1. Visual Representations of Geometric Index Calculations for a Sample Agricultural Field

For the purpose of illustrating how the geometric indices described in Table 1 were calculated for the 4000 agricultural fields, a sample field is considered in this section. Figure 3a–d provide indicative visual representations of the following four geometric indices used to analyze agricultural field shapes; convexity, ellipticity, compactness, and rectangularity. In each plot, the sample field's shape (in blue) is depicted alongside the geometric shape (in green) used to compute the corresponding index. Figure 3a shows the field shape overlaid with its convex hull, illustrating the concept of convexity by comparing the field to its smallest encompassing convex shape. With a convexity value of 0.88, the field's shape is relatively close to its convex hull, indicating a moderately compact shape with some concave indentations. Figure 3b demonstrates the fitting of an ellipse to the field,

indicating how closely the field shape approximates an ellipse. A value of 0.5 suggests that the field is moderately elliptical, with equal tendencies towards being elliptical and irregular. In Figure 3c, the compactness of the field is visualized by comparing it to an equivalent circle with the same area, revealing how tightly or loosely the shape conforms to a circle. Similarly to ellipticity, a compactness value of 0.5 indicates that the field is equally balanced between being circular and non-circular. Finally, Figure 3d shows the field with its minimum bounding rectangle, in terms of calculating the rectangularity index. A value of 0.79 shows that the field is somewhat rectangular, with some deviations from a perfect rectangle, suggesting irregularities in the field's shape.

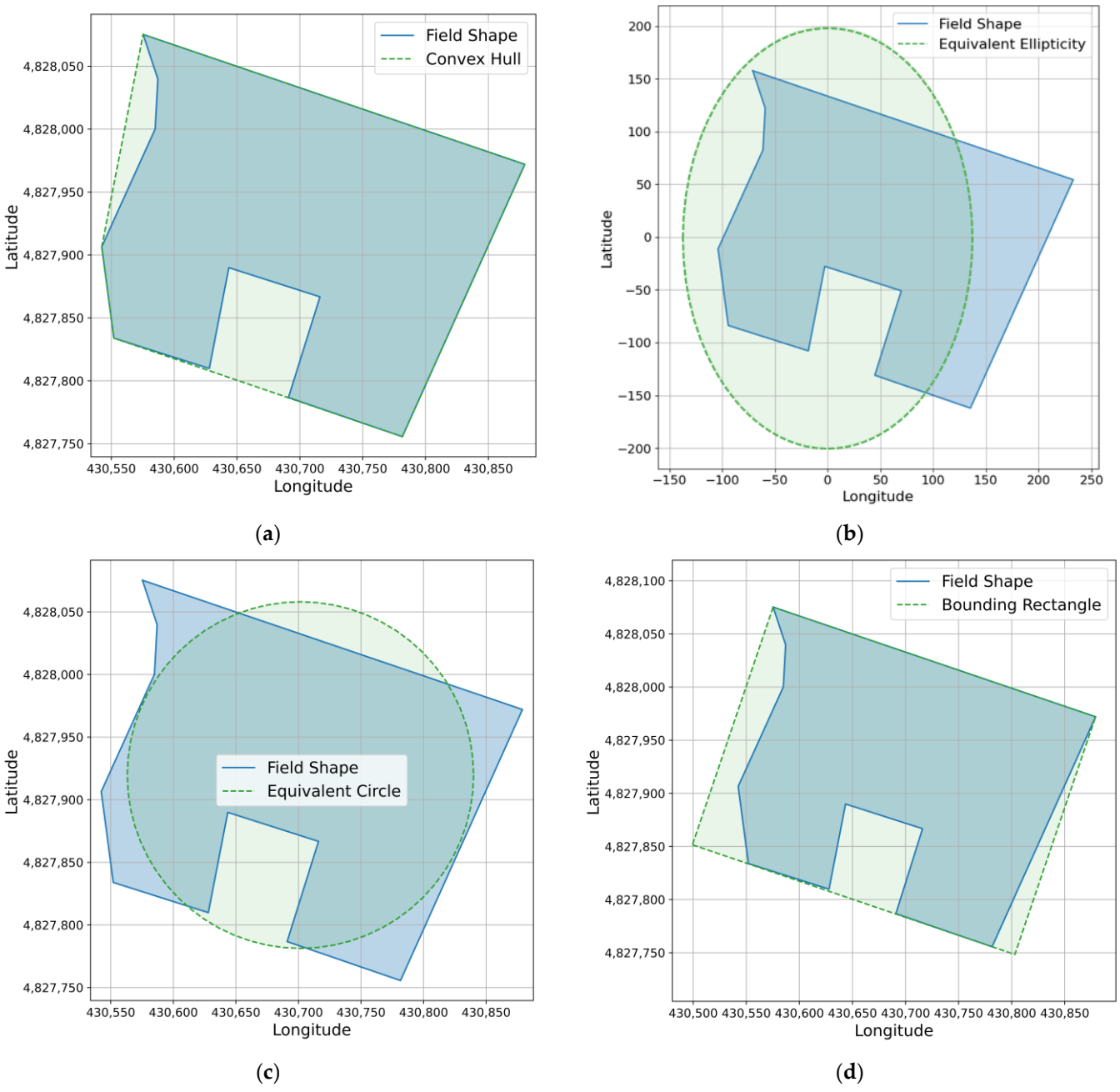

Figure 3. Visual representations of geometric indices for a sample agricultural field: (**a**) convexity, calculated convexity = 0.88; (**b**) ellipticity, calculated ellipticity = 0.5; (**c**) compactness, calculated compactness = 0.5; and (**d**) rectangularity, calculated rectangularity = 0.79.

Figure 4 illustrates the concept of calculating the curb index, as the total field area is compared with the field area after excluding the headlands. The part of the map that encompasses the headlands is colored in green, while the inner polygon is outlined in blue. In this example, the curb index value is 0.26, indicating that the headlands do not play a significant role in the efficiency of these field operations, implying that the field is efficiently utilized, with minimal loss due to boundary effects. Finally, for this sample field, the perimeter-to-area ratio and square-perimeter indices are equal to 0.0204 and 1.252, respectively. The low value of the former suggests that the field has a relatively smooth boundary with low complexity, while the value of the latter indicates minor irregularities or elongations.

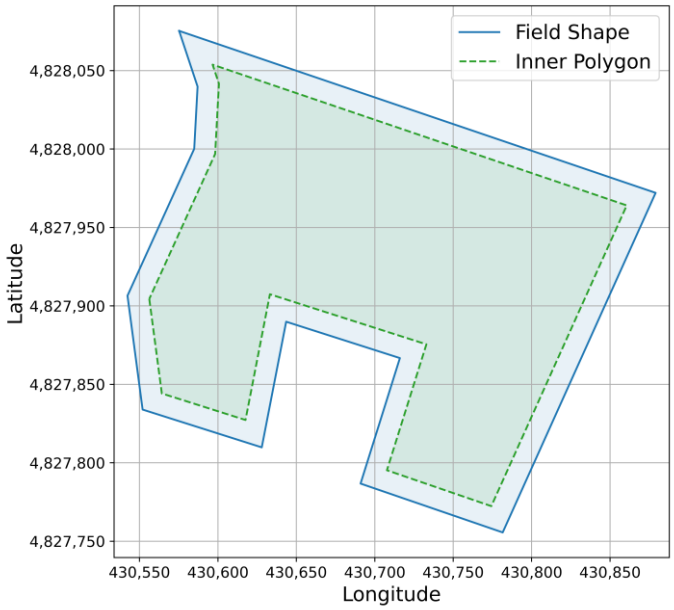

Figure 4. Visualization of the field's boundary and its corresponding inner polygon, calculated Curb Index = 0.26.

3.2. Machine Learning Algorithm Performance Comparison

In this section, we will examine how the ML algorithms fit both the training and test data to assess the models' ability to generalize, as a model which fits the training data well but fails on the test data may be overfitting. This means that it has learned specific patterns in the training set which do not apply to unseen data.

First, the seven ML algorithms were evaluated using the ME, MAE, MSE, RMS, $nRMS$, and R^2 metrics, which are defined in Section 2.5.2. Table 3 summarizes the initial evaluation of each algorithm after training. In short, all the errors for GBR are relatively small, with this model achieving the lowest MAE (0.017) and MSE (0.0006), along with the highest R^2 value (0.942), suggesting a strong fit to the data. DTR is another good regressor, performing well with relatively small errors. It has a low MAE (0.019), MSE (0.0009), and a relatively high R^2 (0.883), combined with the lowest RMS (0.023) and $nRMS$ (0.038).

Focusing on the above ML algorithms, both show small negative ME values, indicating a slight tendency to underestimate the target values. GBR marginally outperforms DTR in terms of MAE, suggesting that GBR generally predicts with slightly higher accuracy on average. Both models have similar MSE values, meaning neither model disproportionately penalizes larger errors. DTR has lower RMS and $nRMS$, indicating that it produces comparatively smaller errors on average relative to the scale of the data. However, GBR performs better than DTR in terms of explaining the variance in the data, with a higher R^2

value. This means GBR provides a better overall fit to the data and captures more of the variability in the target values.

Table 3. Initial machine learning algorithms' performance metrics.

Algorithm	*ME*	*MAE*	*MSE*	*RMS*	*nRMS*	R^2
LR	0.000	0.023	0.001	0.031	0.051	0.873
RR	0.003	0.045	0.005	0.069	0.116	0.347
DTR	−0.001	0.019	0.001	0.023	0.038	0.883
RFR	−0.003	0.019	0.001	0.032	0.053	0.837
GBR	−0.002	0.017	0.001	0.029	0.048	0.942
SVR	0.038	0.054	0.004	0.065	0.109	0.413
XGB	−0.004	0.019	0.001	0.033	0.056	0.846

DTR: decision tree regressor; GBR: gradient-boosting regressor; LR: linear regression; RFR: random forest regressor; RR: ridge regression; SVR: support vector regressor; and XGB: XGBoost regressor.

Notable R^2 values were also observed for LR, XGB, and RFR, though these were lower than those of GBR and DTR, with relatively low error metrics. In contrast, SVR and RR underperformed, with higher MAE and MSE and lower R^2 values, indicating less accurate predictions of FTE. Several factors may have contributed to the underperformance of SVR and RR. In brief, SVR is sensitive to outliers in the dataset [35,36]. Specifically, SVR aims to find a hyperplane that best fits the data, and outliers can significantly influence its positioning. Since SVR uses a margin of tolerance within which errors are not penalized, outliers that fall outside this margin can cause substantial deviations in the model's predictions. As a result, SVR might produce less accurate predictions, especially in datasets with noise or extreme values. Regarding RR, a possible reason for its underperformance could be the relatively high regularization strength applied by the L2 penalty. While regularization is typically beneficial to prevent overfitting, it can cause the model to overly constrain its ability to capture meaningful relationships between the input features and the target variable [37]. Furthermore, RR assumes a linear relationship between the features and the target [38], which may not always be the case, leading to poorer performance, as in the present study.

In conclusion, given that the primary objective of this study is to explain the variation in the data and generalize the model, GBR is the optimal choice, despite having slightly higher errors on individual predictions. This conclusion pertains to the initial performance metrics of the ML algorithms. The final benchmark, presented next, is based on cross-validation, which was also performed to evaluate each model's performance across different subsets of the data.

The 5-fold cross-validation that was carried out helped mainly in preventing overfitting [39,40]. Table 4 shows the performance metrics after cross-validation for different ML algorithms, focusing on the mean R^2 and its standard deviation (Std R^2). The mean R^2 reflects the average proportion of variance explained by the model across different folds, while the standard deviation indicates the variability in performance. Again, GBR stands out, with the highest mean R^2 of 0.931 and a relatively low standard deviation of 0.032, indicating strong and consistent performance across the folds. RFR and XGB also performed well, both having a mean R^2 equal to 0.845 and low standard deviations. On the other hand, RR and SVR demonstrated low mean R^2 values (0.263 and 0.324, respectively), indicating again poor performance.

Table 4. Machine learning algorithms' performance metrics after cross-validation.

Algorithm	Mean R^2	Std R^2
LR	0.802	0.033
RR	0.263	0.236
DTR	0.687	0.199
RFR	0.845	0.049
GBR	0.931	0.032
SVR	0.324	0.100
XGB	0.845	0.077

DTR: decision tree regressor; GBR: gradient-boosting regressor; LR: linear regression; RFR: random forest regressor; RR: ridge regression; SVR: support vector regressor; and XGB: XGBoost regressor.

Overall, taking into account Tables 3 and 4, GBR not only fits the training data well but also generalizes effectively across different subsets, making it a robust choice in terms of prediction of the average FTE. As an ensemble method, it builds multiple decision trees sequentially, correcting previous errors, which helps it effectively model non-linear relationships and handle noise and variability [41,42], often present in real-world agricultural data. The cross-validation employed in this analysis highlights the importance of not solely relying on initial performance metrics. It is also important to consider how well a model generalizes across different data subsets [43]. A representative example in this analysis was the DTR algorithm, which, although it initially had R^2 = 0.883, cross-validation reduced the R^2 to 0.687. This reduction suggests that the DTR model was likely overfitting, learning specific patterns within the training data which did not generalize well when applied to different subsets. Cross-validation revealed this discrepancy, stressing the importance of using techniques such as this one which prevent overfitting.

3.3. Field Traversing Efficiency Prediction Across Different Geographical Regions

3.3.1. Accuracy Assessment of Gradient-Boosting Regressor Against Analytical Approach

For each region (Limburg, The Netherlands; Monsanto, Portugal; Crete, Greece; Peloponnese, Greece; Magnesia, Greece; Indiana, USA; and Aarhus, Denmark), the average FTE was estimated with both the best ML regression algorithm (namely, GBR in this analysis) and analytical method (from Equation (1), provided by Zhou et al. [24]). Figure 5 compares the predicted average FTEs to average FTEs calculated through the analytical method for various locations. Each data point corresponds to a specific region, which is labeled on the plot, while the blue line represents the "ideal fit". The closer the data points are to this line, the better the model's predictions. The scatter plot showcases the strong correlation between predicted and analytical method-based average FTEs, indicating that the model is generally accurate. Nevertheless, there are a few cases where the GBR predictions deviate from the actual values. These are highlighted below.

Table 5 quantifies the above comparison by showing the corresponding percentage error for each case:

$$\text{Percentage Error } (\%) = \frac{|\text{FTE from GBR} - \text{FTE from Equation } (1)|}{\text{FTE from Equation } (1)} \times 100. \quad (8)$$

In total, the GBR model shows a relatively high accuracy in predicting the average FTE, with percentage errors generally being quite small. The errors range from 0.11% to 2.02%, indicating that the GBR model provides predictions close to those calculated by Equation (1). The smallest errors were observed for the fields in Aarhus, Denmark (0.11%), and Magnesia, Greece (0.12%), whereas the largest errors were found for the fields in Crete, Greece (1.86%), and Peloponnese, Greece (2.02%). As can be noticed in Figure 2, the fields presenting the smallest errors have regular shapes, like square, rectangle, and

standard [44], rendering our approach more efficient. Similarly, small errors exist for the fields of Limburg, The Netherlands (0.37%), and Indiana, USA (0.42%). On the other hand, larger errors are associated with more complex shapes, like re-entrant and building plots [44]. However, errors between the analytical and the present ML-based approach are relatively low, reflecting that the GBR algorithm remains effective in predicting FTE, even with some degree of variation.

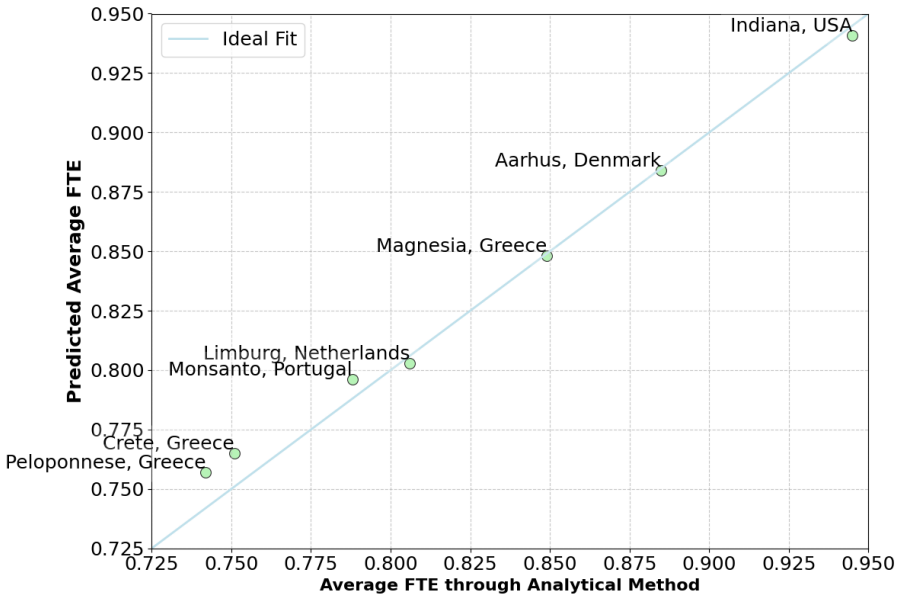

Figure 5. Scatter plot showing the comparison of predicted (via gradient-boosting regressor) and actual average field traversing efficiencies (via Equation (1)) for each geographical region.

Table 5. Accuracy assessment of gradient-boosting regressor in predicting field traversing efficiency (FTE) across different geographical regions.

Geographical Region	Average FTE from Analytical Method	Average FTE from GBR	Percentage Error (%)
Limburg, The Netherlands	0.806	0.803	0.37
Monsanto, Portugal	0.788	0.796	1.02
Crete, Greece	0.751	0.765	1.86
Peloponnese, Greece	0.742	0.757	2.02
Magnesia, Greece	0.849	0.848	0.12
Indiana, USA	0.945	0.941	0.42
Aarhus, Denmark	0.885	0.884	0.11

FTE: field traversing efficiency; and GBR: gradient-boosting regressor.

3.3.2. Evaluation of Gradient-Boosting Regressor Execution Time Against Analytical Approach

Although accuracy is important for ensuring that the GBR algorithm provides reliable predictions, computational time is also essential for practical implementation, scalability, and user experience [45,46]. Thus, balancing both aspects ensures that the model meets operational and practical requirements efficiently. Focusing on the present analysis, although calculating the FTE from Equation (1) provided accurate results, the process proved to be time-consuming, particularly when dealing with large datasets. In contrast, the ML-based model achieved a significant reduction in the execution time while reaching reliable accuracy levels. These findings are clearly demonstrated in Figure 6. In this spider chart, the green color corresponds to the execution time of GBR, which is remarkably less than the analytical approach of Zhou et al. [24]. In particular, an average 73.4% reduction in execution time was achieved with the present developed methodology.

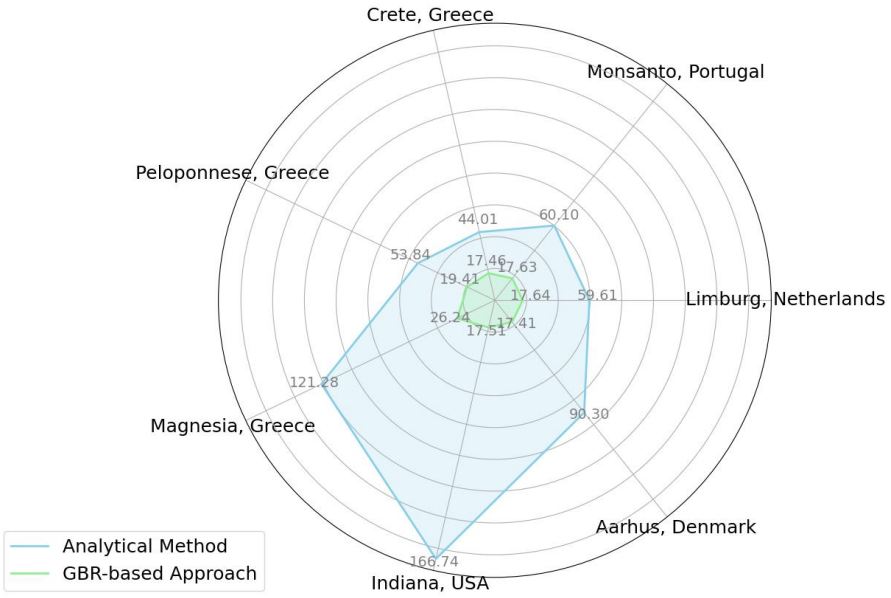

Figure 6. Spider chart illustrating the execution time comparison between the analytical method (via Equation (1)) and the gradient-boosting regressor-based approach for each geographical region.

4. Discussion

Examining ways to enhance FTE can significantly support various aspects of agricultural management [24,25]. By optimizing the use of time, labor, and machinery, efficiency in resource allocation can be accomplished, leading to the minimization of wasted inputs. Furthermore, productivity can be maximized by increasing the output per time unit, improving field coverage, reducing loss time, and accelerating project timelines. These efficiencies can be translated into cost savings and improved operational performance. It enables also the cost-effective scaling of operations, while also extending equipment lifespan by reducing wear and tear. Data-driven insights from FTE can also benefit informed decision making, offering better operational flexibility, risk management, and strategic planning. Environmentally, considering ways to increase FTE can potentially contribute to reducing carbon emissions, minimizing soil compaction and erosion, and decreasing chemical runoff and energy consumption.

However, gathering data about the field geometry, machinery features, and operational patterns necessitates significant resources, while time can also be challenging from a practical point of view. To simplify FTE estimation, an ML-grounded approach was followed in this study, training various ML regression algorithms on scenarios generated from an FMIS [25]. The scope was to significantly simplify the process by relying only on basic geometric indices, rather than requiring detailed operational data. In conclusion, the GBR-based model emerged as the most effective, achieving a high mean R^2 value of 0.931 and consistently low errors. The accuracy of the aforementioned ML model was validated in multiple agricultural fields in Europe and North America, with small percentage errors ranging from 0.11% to 2.02%. The highest accuracy was observed in fields with regular shapes, whereas more complex field shapes led to slightly higher error rates. An R^2 of this magnitude indicated that the chosen geometric indices explained a large proportion (93.1%) of the variability in FTE. Crucially, this study encompassed a substantial dataset of 4000 fields, exhibiting significant variability in shape and size. The fact that a high R^2 was achieved across such a diverse range of field geometries stresses the robustness of the model and its ability to generalize well to different field configurations. This is particularly important because it implies that the model can be applied broadly without needing to be retrained for each specific field shape. This level of accuracy translates to more reliable FTE

predictions, which can be crucial for making informed decisions regarding field operations and resource management. The fact that this high R^2 was achieved using only basic geometric indices, without detailed operational data, and with a significant reduction in computational time compared to the analytical approach highlights this study's success in simplifying FTE estimation. As a consequence, it can be regarded as a reliable tool for estimating FTE in real-world applications, especially when extensive data collection is impractical or time-consuming.

Despite the promising findings of this study, it has some limitations. First, while the present dataset provided a robust basis for model training and validation, it may not fully capture the full spectrum of field shapes, sizes, and operational conditions encountered in global agriculture. The dataset primarily focused on fields in Europe and North America and may not fully represent the diversity of field shapes and sizes found in other regions. Secondly, the model's accuracy is directly tied to the quality and relevance of the chosen indices. Although the selected geometric indices proved effective in this study, exploring additional indices might offer further improvements in predictive accuracy, particularly for complex field geometries. Third, although this study highlighted the efficiency of the GBR algorithm, the computational resources required for training and validation could be a limitation, especially for real-time applications in resource-constrained environments. Finally, while the GBR model provides accurate predictions, its inherent complexity makes it challenging to directly interpret the relationships between the input indices and the predicted FTE.

Future research could focus on expanding the training dataset to include a broader range of field shapes, machinery types, and operational patterns across diverse agricultural environments, while also enhancing model interpretability and transparency through explainable artificial intelligence [47,48]. By improving the understanding of how different features contribute to predictions, farmers and agricultural engineers could gain clearer insights into the model's decision-making process, ultimately fostering trust and facilitating broader adoption of these tools [49,50]. Integrating the present model with other farm management tools and technologies could also provide crucial insights into optimizing their use in real-world scenarios. Collaborative studies including different stakeholders, like agricultural engineers, policymakers, and farmers, could also provide practical feedback towards improving these tools for broader adoption. Another avenue for future work could address the cost implications associated with FTE improvements, as field efficiency is closely linked to the economic performance of agricultural operations [13,28]. For instance, the relationship between initial investments in automated agricultural machineries and long-term cost savings from improved FTE along with reduced fuel consumption and manual labor could be assessed. Finally, incorporating sustainability metrics into FTE models, such as carbon emissions and soil conservation, could support the growing demand for sustainable farming practices that align with environmental goals [51–53].

5. Conclusions

This study demonstrates the potential of ML, specifically GBR, to accurately predict FTE across diverse agricultural landscapes. By relying solely on basic geometric field indices, the GBR model achieved a high R^2 of 0.931, explaining a significant portion of FTE variability. Validated against a large dataset with varying field shapes and sizes across Europe and North America, the model exhibited low prediction errors, with larger errors primarily observed in fields with complex geometries. Critically, the above accuracy was achieved without the need for detailed operational data, providing a practical solution for farmers and agricultural managers who face data collection challenges. Moreover, the GBR approach offers significant computational advantages, reducing execution time by 73.4%

compared to the analytical approach, enhancing scalability and real-world applicability. Future research could expand the dataset to include a broader range of field shapes, machinery types, and operational data, improve model interpretability, and explore the economic and sustainability implications of FTE optimization through interdisciplinary studies.

Author Contributions: Conceptualization, G.A. and D.B.; methodology, G.A., L.B., P.B., C.A. and D.B.; software, G.A. and D.K.; validation, P.B., L.B. and D.K.; formal analysis, C.G.S., S.P. and D.B.; investigation, G.A., L.B., P.B. and C.A.; resources, D.B.; data curation, G.A., C.A. and P.B.; writing—original draft preparation, G.A. and L.B.; writing—review and editing, D.K., C.G.S., S.P., C.A. and D.B.; visualization, G.A. and L.B.; and supervision, D.B. All authors have read and agreed to the published version of the manuscript.

Funding: This research received no external funding.

Data Availability Statement: The original contributions presented in this study are included in the article. Further inquiries can be directed to the corresponding authors.

Conflicts of Interest: Authors Gavriela Asiminari and Dionysis Bochtis are employed by company farmB Digital Agriculture S.A. They declare that this research was conducted in the absence of any commercial or financial relationships that could be construed as potential conflicts of interest.

References

1. Bettucci, F.; Sozzi, M.; Benetti, M.; Sartori, L. A data-driven approach to agricultural machinery working states analysis during ploughing operations. *Smart Agric. Technol.* **2024**, *8*, 100511. [CrossRef]
2. Höffmann, M.; Patel, S.; Büskens, C. Optimal guidance track generation for precision agriculture: A review of coverage path planning techniques. *J. F. Robot.* **2024**, *41*, 823–844. [CrossRef]
3. Jeon, C.-W.; Kim, H.-J.; Yun, C.; Han, X.; Kim, J.H. Design and validation testing of a complete paddy field-coverage path planner for a fully autonomous tillage tractor. *Biosyst. Eng.* **2021**, *208*, 79–97. [CrossRef]
4. Wang, M.; Niu, C.; Wang, Z.; Jiang, Y.; Jian, J.; Tang, X. Study on Path Planning in Cotton Fields Based on Prior Navigation Information. *Agriculture* **2024**, *14*, 2067. [CrossRef]
5. Höffmann, M.; Patel, S.; Büskens, C. Optimal Coverage Path Planning for Agricultural Vehicles with Curvature Constraints. *Agriculture* **2023**, *13*, 2112. [CrossRef]
6. Chakraborty, S.; Elangovan, D.; Govindarajan, P.L.; ELnaggar, M.F.; Alrashed, M.M.; Kamel, S. A Comprehensive Review of Path Planning for Agricultural Ground Robots. *Sustainability* **2022**, *14*, 9156. [CrossRef]
7. Oksanen, T. Estimating operational efficiency of field work based on field shape. *IFAC Proc. Vol.* **2013**, *46*, 202–206. [CrossRef]
8. Bochtis, D.D.; Sørensen, C.G. The vehicle routing problem in field logistics part I. *Biosyst. Eng.* **2009**, *104*, 447–457. [CrossRef]
9. Oksanen, T.; Visala, A. Coverage path planning algorithms for agricultural field machines. *J. F. Robot.* **2009**, *26*, 651–668. [CrossRef]
10. Luck, J.; Zandonadi, R.; Shearer, S. A Case Study to Evaluate Field Shape Factors for Estimating Overlap Errors with Manual and Automatic Section Control. *Trans. ASABE Am. Soc. Agric. Biol. Eng.* **2011**, *54*, 1237–1243. [CrossRef]
11. American Society of Agricultural and Biological Engineers. *Agricultural Machinery Management*; ASABE: St. Joseph, MI, USA, 2015.
12. Palmer, R.J.; Wild, D.; Runtz, K. Improving the Efficiency of Field Operations. *Biosyst. Eng.* **2003**, *84*, 283–288. [CrossRef]
13. Li, Y.L.; Yi, S.P. Improving the efficiency of spatially selective operations for agricultural robotics in cropping field. *Span. J. Agric. Res.* **2013**, *11*, 56–64. [CrossRef]
14. Grisso, R.B.; Cundiff, J.S.; Webb, E.G. Predicting Field Efficiency of Round-Baling Operations in High-Yielding Biomass Crops. *AgriEngineering* **2020**, *2*, 447–457. [CrossRef]
15. Al-Amin, A.K.M.A.; Lowenberg-DeBoer, J.; Franklin, K.; Behrendt, K. Economics of field size and shape for autonomous crop machines. *Precis. Agric.* **2023**, *24*, 1738–1765. [CrossRef]
16. Lampridi, M.G.; Kateris, D.; Vasileiadis, G.; Marinoudi, V.; Pearson, S.; Sørensen, C.G.; Balafoutis, A.; Bochtis, D. A Case-Based Economic Assessment of Robotics Employment in Precision Arable Farming. *Agronomy* **2019**, *9*, 175. [CrossRef]
17. Jensen, T.A.; Antille, D.L.; Tullberg, J.N. Improving On-farm Energy Use Efficiency by Optimizing Machinery Operations and Management: A Review. *Agric. Res.* **2024**, *14*, 15–33. [CrossRef]
18. Kumar, S.; Noori, M.T.; Pandey, K.P. Performance characteristics of mode of ballast on energy efficiency indices of agricultural tyre in different terrain condition in controlled soil bin environment. *Energy* **2019**, *182*, 48–56. [CrossRef]
19. Peura, M.; Iivarinen, J. Efficiency of simple shape descriptors. In Proceedings of the 3rd International Workshop on Visual Form, Capri, Italy, 28–30 May 1997; Volume 5, pp. 443–451.

20. Griffel, L.M.; Vazhnik, V.; Hartley, D.S.; Hansen, J.K.; Roni, M. Agricultural field shape descriptors as predictors of field efficiency for perennial grass harvesting: An empirical proof. *Comput. Electron. Agric.* **2020**, *168*, 105088. [CrossRef]
21. Amiama, C.; Lema, J.; Pereira, J. Prediction of Effective Field Capacity in Forage Harvesting and Disk Harrowing Operations. *Trans. ASABE* **2010**, *53*, 1739–1745. [CrossRef]
22. Gonzalez, X.P.; Alvarez, C.J.; Crecente, R. Evaluation of land distributions with joint regard to plot size and shape. *Agric. Syst.* **2004**, *82*, 31–43. [CrossRef]
23. Zandonadi, R.; Luck, J.; Stombaugh, T.; Shearer, S. Evaluating field shape descriptors for estimating off-target application area in agricultural fields. *Comput. Electron. Agric.* **2013**, *96*, 217–226. [CrossRef]
24. Zhou, K.; Bochtis, D.; Jensen, A.L.; Kateris, D.; Sørensen, C.G. Introduction of a new index of field operations efficiency. *Appl. Sci.* **2020**, *10*, 329. [CrossRef]
25. Asiminari, G.; Moysiadis, V.; Kateris, D.; Busato, P.; Wu, C.; Achillas, C.; Sørensen, C.; Pearson, S.; Bochtis, D. Integrated Route-Planning System for Agricultural Robots. *AgriEngineering* **2024**, *6*, 657–677. [CrossRef]
26. Araújo, S.O.; Peres, R.S.; Ramalho, J.C.; Lidon, F.; Barata, J. Machine Learning Applications in Agriculture: Current Trends, Challenges, and Future Perspectives. *Agronomy* **2023**, *13*, 2976. [CrossRef]
27. Cravero, A.; Pardo, S.; Sepúlveda, S.; Muñoz, L. Challenges to Use Machine Learning in Agricultural Big Data: A Systematic Literature Review. *Agronomy* **2022**, *12*, 748. [CrossRef]
28. Oksanen, T. Shape-describing indices for agricultural field plots and their relationship to operational efficiency. *Comput. Electron. Agric.* **2013**, *98*, 252–259. [CrossRef]
29. Zhou, K.; Leck Jensen, A.; Bochtis, D.D.; Sørensen, C.G. Simulation model for the sequential in-field machinery operations in a potato production system. *Comput. Electron. Agric.* **2015**, *116*, 173–186. [CrossRef]
30. Sharma, P.; Dadheech, P.; Aneja, N.; Aneja, S. Predicting Agriculture Yields Based on Machine Learning Using Regression and Deep Learning. *IEEE Access* **2023**, *11*, 111255–111264. [CrossRef]
31. Elbasi, E.; Zaki, C.; Topcu, A.E.; Abdelbaki, W.; Zreikat, A.I.; Cina, E.; Shdefat, A.; Saker, L. Crop Prediction Model Using Machine Learning Algorithms. *Appl. Sci.* **2023**, *13*, 9288. [CrossRef]
32. Surabhi Lingwal, K.K.B.; Singh, M. A novel machine learning approach for rice yield estimation. *J. Exp. Theor. Artif. Intell.* **2024**, *36*, 337–356. [CrossRef]
33. Ngugi, H.N.; Akinyelu, A.A. Machine Learning and Deep Learning for Crop Disease Diagnosis: Performance Analysis and Review. *Agronomy* **2024**, *14*, 3001. [CrossRef]
34. Niculae, A.; Oprea, S.; Alin-gabriel, V.; Adela, B.; Andreescu, A. Assessing the Role of Machine Learning in Climate Research Publications. *Sustainability* **2024**, *16*, 11086. [CrossRef]
35. Ma, J.; Teng, Z.; Tang, Q.; Qiu, W.; Yang, Y.; Duan, J. Measurement Error Prediction of Power Metering Equipment Using Improved Local Outlier Factor and Kernel Support Vector Regression. *IEEE Trans. Ind. Electron.* **2022**, *69*, 9575–9585. [CrossRef]
36. Shan, X.; Zhang, Z.; Li, X.; Xie, Y.; You, J. Robust Online Support Vector Regression with Truncated ε-Insensitive Pinball Loss. *Mathematics* **2023**, *11*, 709. [CrossRef]
37. Šinkovec, H.; Heinze, G.; Blagus, R.; Geroldinger, A. To tune or not to tune, a case study of ridge logistic regression in small or sparse datasets. *BMC Med. Res. Methodol.* **2021**, *21*, 199. [CrossRef]
38. Meng, W.; He, C.; Zhou, Z.; Li, Y.; Chen, Z.; Wu, F.; Kou, H. Application of the ridge regression in the back analysis of a virgin stress field. *Bull. Eng. Geol. Environ.* **2021**, *80*, 2215–2235. [CrossRef]
39. Allgaier, J.; Pryss, R. Cross-Validation Visualized: A Narrative Guide to Advanced Methods. *Mach. Learn. Knowl. Extr.* **2024**, *6*, 1378–1388. [CrossRef]
40. Belkin, M.; Hsu, D.; Ma, S.; Mandal, S. Reconciling modern machine-learning practice and the classical bias–variance trade-off. *Proc. Natl. Acad. Sci. USA* **2019**, *116*, 15849–15854. [CrossRef]
41. Kazemi, F.; Özyüksel Çiftçioğlu, A.; Shafighfard, T.; Asgarkhani, N.; Jankowski, R. RAGN-R: A multi-subject ensemble machine-learning method for estimating mechanical properties of advanced structural materials. *Comput. Struct.* **2025**, *308*, 107657. [CrossRef]
42. Velthoen, J.; Dombry, C.; Cai, J.-J.; Engelke, S. Gradient boosting for extreme quantile regression. *Extremes* **2023**, *26*, 639–667. [CrossRef]
43. Montesinos López, O.A.; Montesinos López, A.; Crossa, J. Overfitting, Model Tuning, and Evaluation of Prediction Performance. In *Multivariate Statistical Machine Learning Methods for Genomic Prediction*; Springer International Publishing: Cham, Switzerland, 2022; pp. 109–139. ISBN 978-3-030-89010-0.
44. Witney, B. *Choosing & Using Farm Machines*; Longman Higher Education: Essex, UK, 1988.
45. Tonle, F.B.N.; Niassy, S.; Ndadji, M.M.Z.; Tchendji, M.T.; Nzeukou, A.; Mudereri, B.T.; Senagi, K.; Tonnang, H.E.Z. A road map for developing novel decision support system (DSS) for disseminating integrated pest management (IPM) technologies. *Comput. Electron. Agric.* **2024**, *217*, 108526. [CrossRef]

46. Hundal, G.S.; Laux, C.M.; Buckmaster, D.; Sutton, M.J.; Langemeier, M. Exploring Barriers to the Adoption of Internet of Things-Based Precision Agriculture Practices. *Agriculture* **2023**, *13*, 163. [CrossRef]
47. Hassija, V.; Chamola, V.; Mahapatra, A.; Singal, A.; Goel, D.; Huang, K.; Scardapane, S.; Spinelli, I.; Mahmud, M.; Hussain, A. Interpreting Black-Box Models: A Review on Explainable Artificial Intelligence. *Cognit. Comput.* **2024**, *16*, 45–74. [CrossRef]
48. Benos, L.; Tsaopoulos, D.; Tagarakis, A.C.; Kateris, D.; Busato, P.; Bochtis, D. Explainable AI-Enhanced Human Activity Recognition for Human–Robot Collaboration in Agriculture. *Appl. Sci.* **2025**, *15*, 650. [CrossRef]
49. Baron, S. Trust, Explainability and AI. *Philos. Technol.* **2025**, *38*, 4. [CrossRef]
50. Ha, T.; Kim, S. Improving Trust in AI with Mitigating Confirmation Bias: Effects of Explanation Type and Debiasing Strategy for Decision-Making with Explainable AI. *Int. J. Hum. Comput. Interact.* **2024**, *40*, 8562–8573. [CrossRef]
51. Guo, L.; Zhao, S.; Song, Y.; Tang, M.; Li, H. Green Finance, Chemical Fertilizer Use and Carbon Emissions from Agricultural Production. *Agriculture* **2022**, *12*, 313. [CrossRef]
52. Konefal, J.; de Olde, E.M.; Hatanaka, M.; Oosterveer, P.J.M. Signs of agricultural sustainability: A global assessment of sustainability governance initiatives and their indicators in crop farming. *Agric. Syst.* **2023**, *208*, 103658. [CrossRef]
53. Castellini, M.; Diacono, M.; Gattullo, C.E.; Stellacci, A.M. Sustainable Agriculture and Soil Conservation. *Appl. Sci.* **2021**, *11*, 4146. [CrossRef]